Exp Astron (2011) 30:149–164
DOI 10.1007/s10686-011-9213-x

ORIGINAL ARTICLE

Fresnel imager testbeds: setting up, evolution, and first images

Jean-Pierre Rivet · Laurent Koechlin · Truswin Raksasataya · Paul Deba · René Gili

Received: 12 July 2010 / Accepted: 5 January 2011 / Published online: 12 May 2011

Abstract The Fresnel Diffractive Array Imager (FDAI) is a new optical concept proposed for large telescopes in space. To evaluate its performance on real sky objects, we have built a new testbed of FDAI, especially designed for on-sky operation. It is an evolution of the laboratory setup previously used to validate the concept on artificial sources. In order to observe celestial objects, this new two-module testbed was installed in July 2009 at *Observatoire de la Côte d'Azur* (Nice, France). The two modules of the testbed (the Fresnel array module and the receiver module), were secured at both ends of the 19 m long tube of an historical refractor, used as an optical bench on an equatorial mount. In this article, we focus on the evolution steps from a laboratory experiment to the first observation prototype, and on the targets chosen for performance assessment. We show the first on-sky results of a FDAI, although they do not reflect the nominal performances of the final testbed. These nominal performances have been attained only with the latest and most sophisticated prototype, and are presented in a separate article in this special issue.

Keywords Diffractive focussing · Formation flying · High angular resolution · High dynamic range · UV domain · Exoplanets

J.-P. Rivet (✉) · R. Gili
Département Cassiopée, Université de Nice Sophia-Antipolis, CNRS,
Observatoire de la cote d'Azur, B.P. 4229, 06304 NICE Cedex 4, France
e-mail: Jean-Pierre.Rivet@oca.eu

L. Koechlin · T. Raksasataya · P. Deba
Laboratoire d'Astrophysique de Toulouse-Tarbes, Université de Toulouse, CNRS,
14 avenue Edouard Belin, 31400 Toulouse, France

1 Introduction

The concept of Fresnel Diffractive Array Imager (FDAI) as a space borne instrument has been proposed by Koechlin et al. [3, 4], for high resolution astronomical imaging. It is based on the Soret rings experiment [9] and is described in detail in other articles in this special issue.

In this article, we describe how we made the transition between the early 116 Fresnel zones laboratory prototype of Fresnel imager (the so called "Generation 1" prototype) to the 696 Fresnel zones fully featured observation instrument (the "Generation 2" prototype). We present the problems encountered, how we solved them, some sky target choices, the first images, and the initial performance assessments.

We started the validation campaign of the Fresnel diffractive imaging in 2005, shortly after the concept of orthogonal laser-carved Fresnel arrays came out. For a preliminary qualitative validation and for demonstration purpose, we have used a 20×20 mm stainless steel array with 40 Fresnel zones from center to corner, lit with a laser diode.

Later on, thanks to a CNES grant, we have started a quantitative laboratory broadband test campaign on a 80×80 mm array with 116 Fresnel zones on its semi-diagonal ("Generation 1" prototype). Its focal length was 23 m at 600 nm and the wavefront quality better than $\lambda/20$ peak-to-peak. This wavefront quality estimate comes from the position accuracy of the laser carving techniques: 5 μm, which is 20 times smaller than the smallest (outermost) individual sub-aperture.

The chromatic correction was achieved by a 16 mm diameter Silica blazed Fresnel lens with 116 zones. Chromatic correction over the whole visible domain has been assessed. In parallel, an end-to-end numerical simulation tool has been developed [6, 7]. A dynamic range of 10^{-6} has been measured with this laboratory setup, which is in good agreement with the numerical simulations [6]. The diffraction pattern we obtained experimentally was also in quantitative agreement with the simulated image. This proves the diffraction-limited imaging capabilities of this instrument.

However, more intermediate steps are required before a space mission can be accepted, based on this novel concept. One of them involves testing the instrument on real celestial sources. This has been done in 2009 and 2010 with the "Generation 2" prototype, which validates the concept in real observing conditions, and also addresses, in reduced size, some of the navigation aspects of a possible future formation flying space mission. To hold this prototype, we had the opportunity to use the historical 76 cm refractor of the *Observatoire de la Côte d'Azur* (Nice, France). This nineteenth century refractor was one of the largest of its time. We did not use the optics of this 17.89 m focal length refractor, but only its tube (as an optical bench), and its German equatorial mount and drive.

The layout and gradual implementation of the Fresnel astronomical imager prototype is described in Sections 2 and 3 along with the problems encountered and the solutions found. The first stellar images, and the first performance assessments are described in Sections 4 and 5.

The high dynamic range results that have been obtained after complete implementation, and their discussion are published as a separate article in this special issue [2].

2 General layout of the Generation 2 prototype

Our Fresnel Imager Generation 2 testbed has been designed to operate in the optical and close IR domains: 650–663 nm (H_α), 650–740 nm, and 740–880 nm, in order to benefit from a low atmospheric diffusion, sky transparency and better seeing. Moreover, given the external geometric constraints (maximum distance between modules), and the manufacturing constraints of the Fresnel array (minimum size of individual sub-apertures), the surface of the entrance pupil scales like the wavelength to the power two. Thus, choosing relatively long wavelengths allows the largest possible aperture for the Fresnel array.

The testbed consists in two independent modules: the “Fresnel array” module placed ahead, which focuses incoming light by diffraction, and the “receiver” module placed 18 m downstream, which corrects and record the focal images. They are both secured on the west side of the 76 cm refractor’s tube, the optical axis of which runs parallel the axis of our experiment.

The “Fresnel array” module holds the primary entrance diffractive array, a thin metal sheet laser-carved with a carefully designed pattern of sub-apertures, inherited from the Soret ring pattern.

On a standard Soret ring array, all ring-shaped sub-apertures have equal surfaces. However, to get better dynamics, some kind of apodization have been introduced on our Fresnel array: the surface of the sub-apertures is smaller near the edges than at the center. Thus, the outermost sub-apertures are thinner than they would be on a standard Soret ring array. Consequently, the main manufacturing constraint (minimum size of sub-apertures) is more stringent than it would be for a standard Soret ring array.

The different assays of Fresnel arrays tested were designed to have less than 18 m focal length at 800 nm. This is the maximum focal length compatible with safe operations, taking into account the length of the refractor’s tube and the inner radius of the dome. Given the maximal focal length of the array, the central wavelength λ_0, and the minimum sub-aperture size $d_{\min}$ compatible with the laser carving technology, we can compute the maximum size of the array, and the corresponding number of Fresnel zones. To do so, we need the following expressions for the focal length F and the size d of the smallest (outermost) sub-aperture:

$$F = \frac{\Phi^2}{8\,k_{\max}\,\lambda} \qquad \text{and} \qquad d = \frac{\Phi}{8\,k_{\max}\,\alpha}, \tag{1}$$

where λ is the corresponding wavelength, Φ is the diagonal size of the square Fresnel array, $k_{\max}$ is the number of Fresnel zones from center to corner, along the diagonal, and α is a coefficient larger than 1, that accounts for the apodization (the smallest sub-aperture is smaller than in the corresponding Soret rings array; $\alpha = 1$ without apodization). Consequently, for a wavelength λ and a targeted focal length F, the expressions for the maximum diagonal size Φ and the maximum number $k_{\max}$ of Fresnel zones read:

$$\Phi_{\max} = \frac{F\,\lambda}{\alpha\, d_{\min}} \qquad \text{and} \qquad n_{\max} = \frac{F\,\lambda}{8\alpha^2\, d_{\min}^2}, \tag{2}$$

where $d_{\min}$ is the minimum achievable sub-aperture size. Taking into account the manufacturing limitation (no carving smaller than = 20 μm) and the focal length limitation at 18 m, we chose to design a 200 × 200 mm square aperture Fresnel array ($\Phi = 283$ mm) with 696 Fresnel zones on the semi-diagonal. The resulting focal length at $\lambda_0 = 800$ nm is $F_0 = 17.96$ m.

The Fresnel array is mounted on a mechanical frame which allows for manual rotations around the optical axis. This is useful to reject the diffraction spikes in regions of the image where they do not hide astronomically relevant elements.

The "receiver module" is more complex. It incorporates a field optics with a field stop, and a precision blazed Fresnel lens to compensate for the chromatism of the primary Fresnel array (focal length proportional to λ^{-1}). This fine optical component must be located in a plane where the field optics produces a sharp image of the entrance Fresnel array.

As any diffraction grating, the primary Fresnel array diffracts the incoming light on several diffraction orders. Only the light from the order +1 is focused on the CCD sensor. The light beams from other diffraction orders focus in other planes, and spread onto the sensor, acting as a near uniform background that might hamper the high dynamics capabilities of the imager. Most of these beams are too faint to have a significant contribution at the sensor's level, except the light diffracted at the zero order. This light is not focused at all when it reaches the field optics. Thus, it converges in the focal plane of the field optics. To reject this unwanted light, a 1.5 mm opaque solid circular stop is inserted in this focal plane. This so-called "zero order mask" is held in position by a spider (two crossed 30 μm wires).

The receiver module also incorporates the science and guiding cameras, two *Andor Luca R* EMCCD cameras, and a custom-designed doublet to produce a final image onto the camera's sensor. The resulting effective focal length a the detector plane is $f = 3.12$ m.

Finally, for the sake of image dynamics and sharpness, the Generation 2 prototype incorporates a tip-tilt corrector. Its goal is to reduce the impact of the mechanical defects of the mount, and also of the lowest orders of the atmospheric turbulence.

The distance between modules is fixed, but the receiver module's orientation is steerable by a remote controlled two-axis translation stage. This attitude control is necessary for a precise alignment of both modules. This alignment condition is crucial for an accurate chromatic correction: the image of the entrance Fresnel array through the field optics must coincide exactly with the blazed Fresnel lens. Due to mechanical flexions, the attitude of the receiver module has to be fine-tuned frequently.

The angular on-sky field is limited by the diameter $D = 45$ mm of the field stop located at the entrance of the field optics. With a focal length of $F_0 = 17.96$ m at the central wavelength $\lambda_0 = 800$ nm, this leads to a monochromatic field of view $\theta_0 = 517''$. For a non-vanishing bandpass $\Delta\lambda$, there is a trade-off between the field of view and the bandpass, for a given size of the field stop. Indeed, wavelengths longer than the nominal one (λ_0) will converge upstream with respect to the field stop (located at a distance F_0 of the primary Fresnel array). On the contrary, sorter wavelengths will converge downstream. Consequently the input beam for non-nominal wavelengths will have a non-vanishing size at the level of the field stop. Thus, the broadband unvignetted field of view θ and the bandwidth $\Delta\lambda$ for a given field stop diameter D are linked by the following relation:

$$\theta + \frac{\Phi}{F_0}.\frac{\Delta\lambda}{2\lambda_0} = \frac{D}{F_0} = \theta_0, \tag{3}$$

where Φ is the diagonal size of the square entrance Fresnel array and F_0 is the primary focal length at the nominal wavelength λ_0. On our Generation 2 prototype, the maximum unvignetted bandwidth for vanishing field of view is thus $\Delta\lambda_{\max} = 254$ nm for $\lambda_0 = 800$ nm.

In space, as the focal length will correspond to the distance between two free flying spacecraft (a few kilometers), Fresnel arrays will not suffer this limit in focal length, hence in aperture. However, large apertures will imply relatively large field optics: the field optics diameter being 1/6 to 1/10 of the primary aperture diameter (e.g. 0.4 m to 0.6 m prime focus field for a 4 m aperture). The other optics, downstream in the receptor module will be much smaller, and the corresponding ones in our Generation 2 testbed have diameters about half of those of a 4 m space borne Fresnel imager.

For a square aperture Fresnel array of size C, the angular resolution is the same as that of a solid square aperture: $R_{Airy} = \lambda/C$. The Rayleigh resolution

Table 1 Specifications of the full-fledged Fresnel imager Generation 2 testbed

Fresnel array size	200×200 mm
Number of Fresnel zones from center to corner	696
Type of Fresnel array	Orthocircular (Serre et al., 2009)
Central wavelength λ_0	800 nm
Primary focal length F_0 at λ_0	17.96 m
Field stop diameter	45 mm
Field of view for vanishing bandwidth θ_0	$517''$
Unvignetted bandpass $\Delta\lambda_{\max}$ for vanishing field of view	673–927 nm
Angular airy radius at λ_0	$0.825''$
Detector pixel size	8 μm
Final focal length f (at detector)	3.12 m
Pixels per airy radius	1.5

for the Generation 2 prototype is $0.825''$. Since the CCD sensor has 1,000 × 1,000 pixels of 8 × 8 μm (0.53 × 0.53" for a final focal length $f = 3.12$ m), the final image contains roughly 650 × 650 resolution elements.

The specifications of the Generation 2 ground-based testbed are summarized in Table 1.

3 Gradual evolution from Generation 1 to Generation 2

From the laboratory Generation 1 prototype to the full-fledged sky-watcher Generation 2 instrument, we chose to evolve in a step by step approach, new components replacing the old ones gradually, while keeping the optical system operational. On-sky validations were performed after each significative upgrade of the instrument. The major milestones between the early laboratory testbed and the latest on-sky instrument are summarized in Table 2. Figures 1 and 2 show the primary Fresnel arrays of Generation 1 and Generation 2 testbeds respectively,

3.1 The "Generation 1.5.1" intermediate prototype

The design phase for the on-sky version lasted from December 2007 to June 2009. We chose the wavelength domain and designed the optics accordingly. The technical solutions to secure the two modules of the testbed onto the refractor's tube were crucial design issues. Standard hardware solutions had to be rejected, since the refractor is part of an historical monument, and no permanent modification was allowed. Nonetheless, the mechanical link between the modules and the refractor's tube had to be as stable and reliable as possible, for the sake of instrumental stability. Another important issue was the logical connection between the refractor's driving electronics and the prototype's tip-tilt corrector device: when the tip-tilt corrector happens to run out of its correction range, it has to automatically interact with the refractor's slow motion driving system.

Table 2 Summary of the technical evolution of the Fresnel imager testbeds from the early Generation 1 prototype to the full-fledged Generation 2 instrument

Generation	1	1.5.1	1.5.2	2
First light	04/2006	06/2009	09/2009	01/2010
Context	Lab.	Sky	Sky	Sky
Primary array size (mm)	80 × 80	200 × 200	200 × 200	200 × 200
Primary array # of zones	116	696	696	696
Fresnel lens diameter (mm)	16	16	58	58
Fresnel lens # of zones	116	116	702	702
Imaging doublet	Off-the-shelf	Off-the-shelf	Custom	Custom
Detector(s)	*Starlight SXV-H9*	*Starlight SXV-H9*	*Starlight SXV-H9*	2× *Andor Luca R*
Tip-tilt corrector	No	No	No	Yes

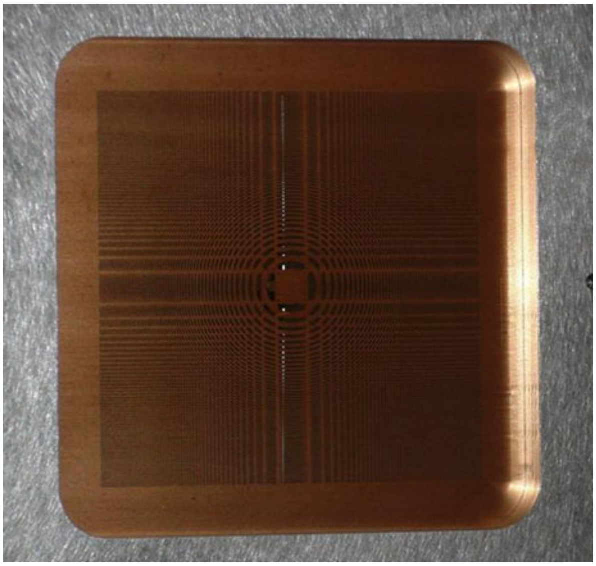

Fig. 1 The primary Fresnel array for the Generation 1 prototype: 80 × 80 mm, 116 Fresnel zones from *center* to *corner*

In spring 2009, a new 200 × 200 mm metal primary array with 696 Fresnel zones was carved by *Micro Usinage Laser* and replaced the 80 × 80 mm array with 116 Fresnel zones, formerly tested in our laboratory setup (Generation 1). The new compound “orthocircular” design [8] for the 200 × 200 mm Fresnel array involves less bars to sustain the Fresnel rings, than the earlier one used on the laboratory Generation 1 testbed. As a consequence, the spikes are 3 times

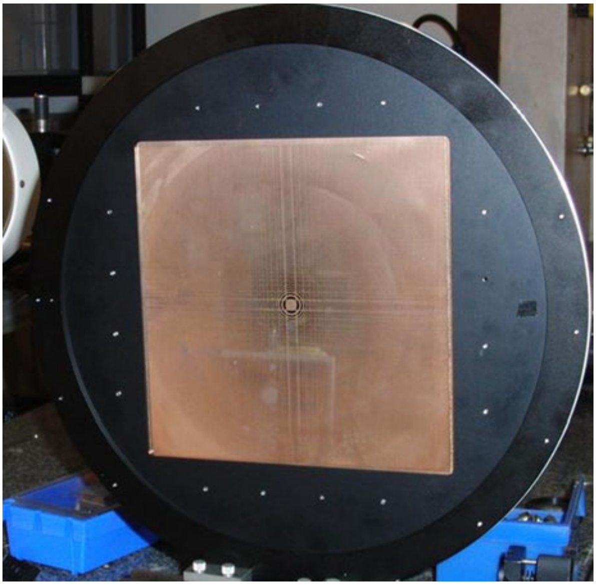

Fig. 2 The primary Fresnel array for the Generation 2 prototype: 200 × 200 mm, 696 Fresnel zones from center to corner

fainter and the central lobe almost twice as bright. Thus the brightness ratio is improved by a factor 6.

The previous chromatic correction Fresnel lens (diameter 16 mm, 116 Fresnel zones) was still in use. This limited the effective aperture to a circle of 115 mm in diameter. The instrument operated without any tip-tilt corrector. Consequently, the atmospheric tip-tilt and the mechanical drifts and flexions affected the quality of the images. The sensor was still a *Starlight SXV-H9* camera (392 × 1,040 pixels of 6.45 × 6.45 μm).

In July 2009 the Generation 1.5.1 testbed was moved on the 76 cm refractor's tube in Nice, and received its first star light. The specifications of this intermediate step is described in the column "Gen. 1.5.1" of Table 2 (the column "Gen. 1" of this table recalls the specification of the early laboratory testbed).

3.2 The "Generation 1.5.2" intermediate prototype

In September 2009, the new 58 mm blazed Fresnel lens with 702 Fresnel zones (manufactured by ion etching on fused silica) is delivered by *SILIOS Technologies*. This Fresnel blazed lens intended for chromatic correction has six more zones on its semi-diagonal than the primary Fresnel diffractive array. This allows for slight displacements of the primary array's image on the blazed Fresnel lens. The slight linear chromatism that results from these displacements is needed to compensate for differential atmospheric chromatism at moderate or high air masses. In addition, a new, custom-designed, doublet was also delivered, for final imaging on the CCD sensor. Special housing had to be designed and realized to protect these fine optics against dust contamination during on-sky operations (no clean room). These new optical elements have sufficient diameter to take advantage of the full 200 × 200 mm of the aperture diffractive Fresnel array.

The mechanical structure of the prototype have also been improved: when not strictly vertical, the 2 m optical rail of the receiver module bends under the effect of gravity. This leads to orientation-dependent internal misalignments within the optical components of the receiver. To cope with this problem, we have stiffen the optical rail of the Generation 1.5.2 prototype with yards and marine-like steel guys.

Besides the flexions of the receiver's optical rail, the 18 m long refractor's tube also bends under the action of gravity. Thus, the tube takes a bow shape, the flexion angle of which can reach a few arc minutes. In normal operation mode (that is, when the instrument is used as a standard refractor), this altitude-dependent bending of the tube does not affect the orientation of the refractor's optical axis, since the tube is designed so that both ends deviate by the same amount. However, as our receiver module is linked to the rear end of the tube, its orientation follows the local tangent to the tube. This yields some altitude-dependent misalignment of the receiver module with respect to the Fresnel array module. Consequently, the correct alignment of both modules, which is critical for correct chromatic correction, has to be checked and corrected frequently. The angular precision required for a good chromatic correction is λ_0/D, where D is the diameter of the field optics. This corresponds to 3.6″ for a 45 mm field stop at 800 nm. The adjustment procedure that we have developed to solve this problem is likely to be helpful to design the policy of attitude control for the receiver spacecraft in future formation flying space borne version.

3.3 The "Generation 2" final prototype

As far as only optical elements are concerned, the Generation 1.5.2 testbed is complete at this stage. However, the quality of long exposure images was hampered by tit-tilt motions of various origins (slight polar misalignments, periodic error of the mount's worm gear, tube mechanical flexions, atmospheric turbulence). In addition, the non-intensified CCD sensor of the *Starlight SXV-H9* camera lacked some sensitivity. These problems have been corrected (at least partially) by a 100 Hz tip-tilt corrector, which was delivered late 2009, together with a new sensor module. This sensor module features two *Andor Luca R* intensified EMCCD cameras, one to record science images, an the other one to monitor tip-tilt errors on a guide star. The beam splitting between both cameras is done by a dichroic plate. A computer closes the servo loop and sends translation orders to the piezoelectric XY translation stage which bears the final imaging doublet. The resulting Generation 2 prototype of Fresnel imager and its first results are thoroughly described in a separate article in this special issue [2].

4 First on-sky images with the Generation 1.5.1 intermediate prototype

The first on-sky images from our Fresnel Imager have been acquired in July 2009 with the Generation 1.5.1 testbed. Several observations of bright single stars and of binary or multiple systems have been done, for performance assessments.

4.1 Bright single stars

Two very bright stars, *Vega* and *Deneb*, have been used for the initial optical alignements of the testbed, and for a careful study of the PSF. As far as we know, these images are the very first images of astronomical targets obtained with a carved metal sheet as focusing component.

Figure 3 shows an image of *Deneb* taken with the Generation 1.5.1. The image displays the four expected spikes in the PSF, due to the orthogonal structure of the bars which hold the Fresnel rings in the diffraction array. Four diffraction spikes stick out from the central lobe of the PSF: two from order (0 in x, $+1$ in y), and two from order ($+1$ in x, 0 in y). The central lobe originates from diffraction order ($+1$ in x, $+1$ in y).

Besides the four expected spikes, four other short spikes show up. They are due to the diffraction of light by the spider holding the zero order mask

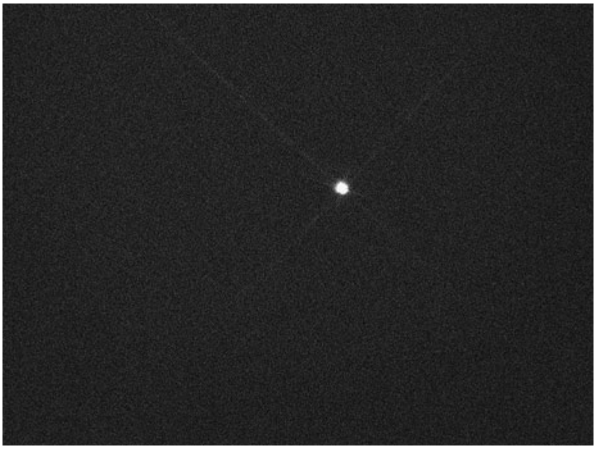

Fig. 3 Image of *Deneb*, with the Generation 1.5.1 testbed in the 740–900 nm bandpass. The central lobe and the diffraction spikes of the primary array are clearly visible. A secondary set of spikes is also visible, originating from diffraction by the spider of the zero order mask

(see Section 2). In later observation runs, the respective orientation of the primary array and of the spider have been trimmed so that both spike sets be superimposed.

4.2 Multiple stars

Tests on multiple stars have been performed for field calibration, and to assess the capabilities of our Fresnel imagers in terms of contrast and effective resolution. Table 3 sums up the characteristics of the double or multiple stars which have been considered in this article. For these tests, the exposure time varies between 1 s and 100 s, and the selected spectral band is 750–850 nm. As a consequence, the V-magnitudes in Table 3 do not reflect exactly the PSF brightness ratios.

Figure 4 shows an image of the $\epsilon - Lyr$ system obtained with the Generation 1.5.1 prototype. Since the effective aperture of this prototype was 115 mm in diameter (see Section 3.1), the expected diffraction-limited resolution is 1.7″ at 800 nm. On the image we obtained, the PSFs are blurred asymmetrically. This is due to a less than ideal chromatic correction stability. The resulting

Table 3 Characteristics (magnitudes and separations) of the binary and multiple systems under consideration in this article

System		V magnitude	Separation
STT 433	A	4.4	
	B	10	A-B: 15.3″
	C	9.9	A-C: 21.8″
$\epsilon_1 - Lyr$	A	5.0	
	B	6.1	A-B: 2.6″
$\epsilon_2 - Lyr$	C	5.2	A-C: 212″
	D	5.5	C-D: 2.3″
STF 2726 (52 − *Cyg*)	A	4.2	
	B	8.7	A-B: 6.4″

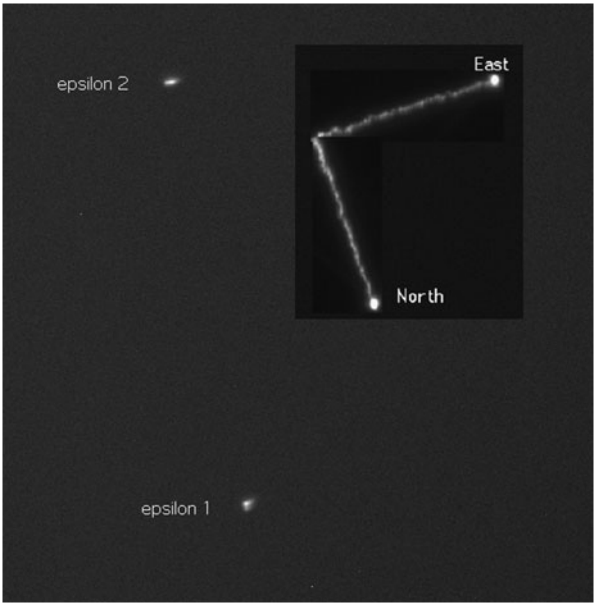

Fig. 4 Image of the multiple system $\epsilon_1 - Lyr$ and $\epsilon_2 - Lyr$ obtained with the Generation 1.5.1 prototype (115 mm effective aperture). The direction of separation of these binary systems are approximately at right angle. On this image, the chromatism is not perfectly corrected, hence the anisotropic blurring of the PSFs. The *upper-right* inserted image shows the north and east directions (see text)

anisotropic PSF size is $2 \times 4''$. Consequently, the two components of $\epsilon_2 - Lyr$ are not clearly resolved, whereas those of $\epsilon_1 - Lyr$ are.

To have the East-West orientation of the pictures, we have made a 10 s exposure on $\alpha - Lyr$, with the sidereal motion switched off (see inserted picture in Fig. 4). The wrinkles on the East-West track are due to atmospheric tip-tilt only, since the refractor's tube was still. This axis orientation holds for star images presented here, made with the *SXV-H9* camera.

The scale of the image, in arc seconds per pixel, can be deduced from a distance measurement on the image, and from the angular separation of the couple. The final focal length on the CCD sensor can be deduced from the Camera's pixel size (6.45 μm for the *SXV-H9* camera). Table 4 sums up this calculation. The resulting scale is $0.372 \pm 0.001''$/pixel. This effective focal length is much shorter than the primary array focal length. This is due to the relay optics (blazed Fresnel lens and imaging doublet) in the receiver module that we have dimensioned for a correct sampling of the PSF. This value is different for the Generation 1.5.2 prototype, since the blazed Fresnel lens is different.

Figure 5 is a long exposure (300 s) image of the binary star STF 2726 ($52 - Cyg$). The companion is 4.5 magnitudes fainter than the central star,

Table 4 Image scale calibration with $\epsilon - Lyr$

Angular separation ($''$)	209.85
Linear separation (px)	564 ± 1
Scale ($''$/px)	0.372 ± 0.001
Focal length (mm)	$3{,}576 \pm 6$

Fig. 5 Image of the double star *STF* 2726 (52 − *Cyg*) obtained with the Generation 1.5.1 prototype (115 mm effective aperture). The companion on the right hand side is 4.5 magnitudes fainter than the *central star*, and separated by 6.4″

and the angular separation is 6.4″. The companion *STF* 2627-B (permutate 26 and 27) emerges out of the noise, on the right side of the main star. The noise clearly visible in the image comes from the lack of sensitivity of the *Sony ICX285AL* CCD sensor of the *SXV-H9* camera. The system *STF* 2726 is the closest couple with such a magnitude difference we have imaged with the Generation 1.5.1 testbed. It is worth noting that this 300 s exposure have been obtained without any guiding or tip-tilt correction. The refractor's mount and drive happen to be accurate enough to allow such 300 s exposures without any correction. As for $\epsilon - Lyr$, the scale of the image can be deduced from a distance measurement on the image, and from the angular separation of the couple, found in the Washington Double Star catalog (WDS). Table 5 sums up this calculation. The resulting scale is 0.38″/pixel. Even with the same optical elements, the effective focal length strongly depends on the exact positions of these elements, and also on the focus setting of the field optics (a Maksutov telescope). This is why the focal length estimate obtained with *STF* 2726 (3.47 m) slightly differs from the value obtained with $\epsilon - Lyr$ (3.58 m). As a consequence, the image scale calibration must be performed after each optical fine tuning operation. In the future, this scale calibration will be done by observing a bright single star with a narrow band filter, through a broad grating

Table 5 Image scale calibration with the binary star *STF* 2726

Angular separation (″)	6.4
Linear separation (px)	16.7
Scale (″/px)	0.38
Focal length (mm)	3,472

located upstream from the primary Fresnel array. This will produce secondary peaks in the image, at precise angles [1].

5 Results obtained with the 1.5.2 intermediate prototype

The triple star STT 433 have been used to assess the high dynamic imaging capabilities of the Generation 1.5.2 testbed (full 200 × 200 mm aperture; new 58 mm blazed Fresnel lens for chromatic correction). Figure 6 shows the resulting image. The spikes appearing on this image have been oriented so that they do not overlap the companion stars. The orientation of the spikes can be trimmed by rotating the main Fresnel array around its optical axis.

To test the imaging capabilities of the Generation 1.5.2 prototype on resolved astronomical sources, we have taken pictures of the Moon (see Fig. 7). This demonstrates the imaging quality of Fresnel imagers on large fields or on fields with a bright background. The contrast is lower than in the case of compact objects, but the high resolution is still there.

For these images of the Moon, the chromatic correction settings have been performed by taking advantage of the moiré fringes that appear in the pupil plane from the superposition of two Fresnel rings patterns: the main array and the blazed Fresnel lens [5]. The orientation and spacing of these moiré fringes give informations on the residual misalignment. In later versions of the prototype, extra optics will be added, to image the pupil plane. So, controlling the correct superposition of the blazed Fresnel lens and of the image of the primary Fresnel array will be made easier and more accurate.

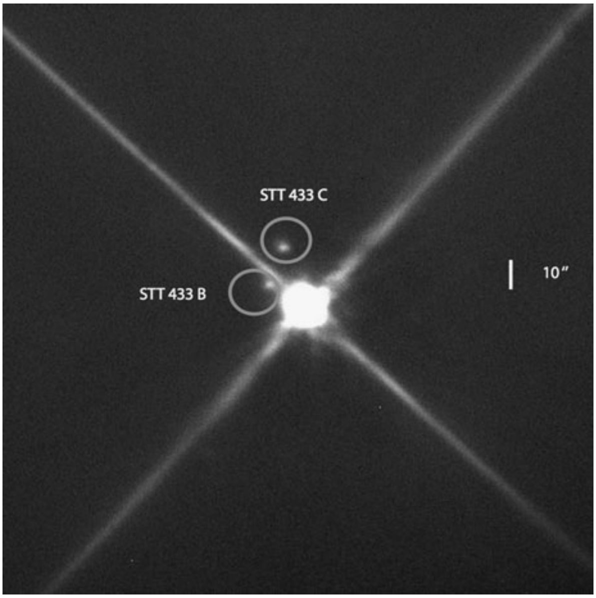

Fig. 6 Image of the multiple star STT 433 and its companions B and C, with the Generation 1.5.2 prototype. Exposure time on the *SXV-H9* camera: 300 s

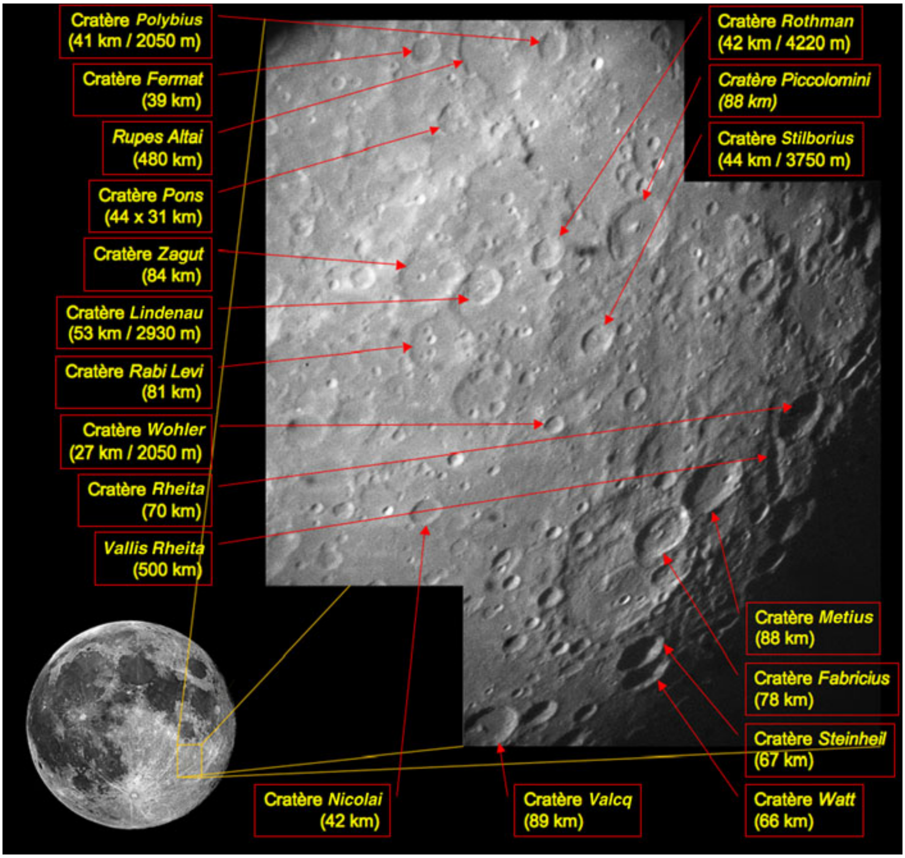

Fig. 7 Mosaic of two images covering 1155 × 986 km on the Moon, obtained with the Generation 1.5.2 prototype on October 7, 2009. The pictures show the south-eastern part of the quasi full moon, between *Nectaris Mare* and *Janssen Highland*

The mosaic of two images in Fig. 7 shows a region in the south-east of the Moon around *Janssen Crater* (45 South, 42 East) and *Reita Vallis*, which extends north-south on 500 km. The bright diagonal strip is a ray from *Tycho Crater*, crossing *Rupes Altai*. The field covered in a single frame is 1,070 × 800 km. The exposure time on the *SXV-H9* CCD camera was 100 ms. The scale calibration of this image has been done on six large and well defined craters clearly visible in the field, assuming a topocentric distance of 372,000 km for the Moon region under consideration, at the date of the observation (October 7th, 2009, 03h UT). We find an average field scale of 0.426″ per pixel, and an effective focal length of 3.12 m for a pixel size of 6.45 µm. Table 6 sums up the calibration measurement on the Moon.

At 800 nm with a 200 × 200 mm aperture, the diffraction-limited resolution is 0.82″. This corresponds to a linear resolution of 1.5 km on the Moon, and 1.94 pixels on the CCD sensor. Kilometric-sized details are visible on the

Table 6 Scale calibration for the image of the Moon

Crater	Zagut	R. Levi	Nicolai	Lindenau	Buch	Büsching	Average
Diameter (km)	84	81	41	53	54	52	
Diameter (″)	47	45	23	29	30	29	
Diameter (pix)	97	106	53	74	72	70	
Scale (″/pix)	0.480	0.423	0.429	0.397	0.416	0.412	0.426

full resolution image of the Moon. For example, the shadow inside the 6 km satellite crater *Nicolai-D* (small crater on the North side of *Nicolai Crater*) is clearly visible. Thus, this image of the Moon obtained with Generation 1.5.2 prototype can be considered as close to diffraction limited.

6 Conclusions and perspectives

The intermediate prototypes 1.5.1 and 1.5.2 have modest performances. They were only intended to reveal the potential problems, to prepare the observation procedures, and to ensure a progressive transition between the laboratory prototype and the final Generation 2 observing testbed. The full performances will be attained with the full Generation 2 prototype, equipped with a tip-tilt correction and with more sensitive EMCCD cameras.

Figure 8 is a separation versus magnitude difference diagram. The star-shaped dots represent the couples actually measured with the intermediate prototypes. The continuous curve is the boundary of the theoretically accessible region, and the shaded elliptic shape sketches the region that is to be sampled by the Generation 2 instrument.

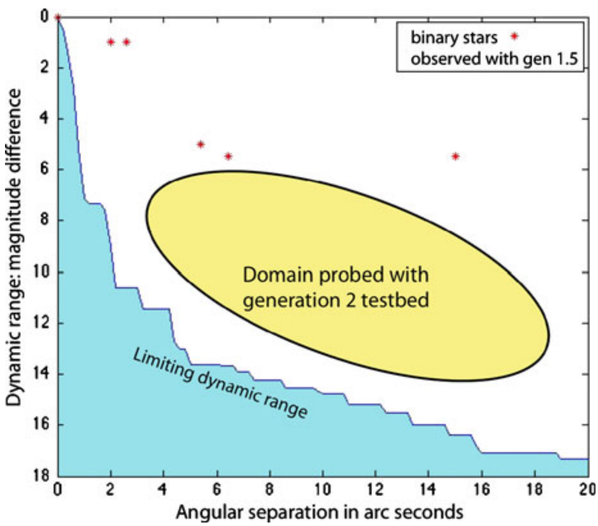

Fig. 8 Separation versus contrast diagram. The *star markers* represent the couples actually studied with the Generation 1.5.1 and 1.5.2 testbeds. The *continuous curve* is the theoretical limit, and the *ovale shaded shape* sketches the expected region of action of the full Generation 2 testbed

The preliminary experiments reported in this article have provided for valuable experimental feedback. For example, they have clearly demonstrated the importance of frequently controlling and correcting the orientation of the receiver module, in order to have a correct chromatic correction.

The mechanical stiffness of the optical rail in the receiver module has also proven to be an important issue. Simple "hardware" solutions have been found, implemented and successfully tested on the intermediate prototypes. This valuable experimental feedback has benefitted to the Generation 2 prototype.

The Generation 2 prototype which is currently under investigation will allow higher dynamic range and resolution observations. Another article in this special issue is dedicated to its first observation campaign during which more difficult targets have been studied.

Acknowledgements This work has been funded by CNES, Université de Toulouse, CNRS, Fondation STAE, and made possible thanks to the involvement of many people at Observatoire Midi Pyrénées and Observatoire de la Côte d'Azur. We are specially thankful to Jacqueline Platzer, Driss Kouach, Bruno Dubois, Marcel Belot, Marin Cortial, Jean-Jacques Bois, Carine Marchive, Thierry Mallet, and the "Service de Mécanique Mutualisé" at the Observatoire de la Côte d'Azur.

References

1. Germain, M.E., Douglass, G.G., Worley, C.E.: Speckle Interferometry at the US Naval Observatory III. Astron. J. **117**, 2511–2527 (1999)
2. Koechlin, L., Rivet, J.-P., Deba, P., Raksasataya, T., Gharsa, T. Gili, R.: Generation 2 testbed of Fresnel imager: first results on the sky. Exp. Astron. (2011). doi:10.1007/s10686-010-9203-4
3. Koechlin, L., Serre, D., Deba, P., Pelló, R., Peillon, C., Duchon, P., Gomez de Castro, A.I., Karovska, M., Désert, J.-M., Ehrenreich, D., Hebrard, G., Lecavelier Des Etangs, A., Ferlet, R., Sing, D., Vidal-Madjar, A.: The fresnel interferometric imager. Exp. Astron. **23**, 379 (2009)
4. Koechlin, L., Serre, D., Duchon, P.: High resolution imaging with fresnel interferometric arrays: suitability for exoplanet detection. Astron. Astrophys. **443**, 709–720 (2005)
5. Mertz, L., Young N.O.: Fresnel transformation of images. In: Habell, K.J. (ed.) Proceedings of the International Conference on Optical Instrumation Techniques, vol. 305. Chapman and Hall, London (1961)
6. Serre, D.: L'Imageur interférométrique de Fresnel: un instrument spatial pour L'observation à Haute Résolution Angulaire. PhD thesis, Université Paul Sabatier, Toulouse, France (2007)
7. Serre, D.: The Fresnel imager: instrument numerical model. Exp. Astron. (2011). doi:10.1007/s10686-010-9200-7
8. Serre, D., Deba, P., Koechlin, L.: Fresnel interferometric imager: ground-based prototype. Appl. Opt. **48**(15), 2811–2820 (2009)
9. Soret, J.-L.: Sur les phénomènes de diffraction produits par les réseaux circulaires. Arch. Sci. Phys. Nat. **52**, 320–337 (1875)